Journal of the Korean Nuclear Society
Volume 31, Number 6, pp.548~560, December 1999

Air-Water Countercurrent Flow Limitation in a Horizontal Pipe Connected to an Inclined Riser

Seong-Kwon Kang, In-Cheol Chu, Hee Cheon NO, and Moon-Hyun Chun
Korea Advanced Institute of Science and Technology
373-1, Kusong-Dong, Yusong-gu, Taejon, 305-701, Korea
bluesky@kepsa.kaist.ac.kr
Chang-Kyung Sung
Korea Electric Power Rescarch Institute
103-16 Munji-Dong, Yusong-gu, Taejon 305-380, Korea

(Received May 29, 1999)

Abstract

An experimental investigation has been performed to examine the effects of various geometrical parameters and an initial operating condition on the air-water countercurrent flow limitation (CCFL) in a simulated PWR hot leg. A total of 118 experimental data for the onset of CCFL and zero liquid penetration were obtained for various combinations of test parameters. It was observed that the CCFL can be classified into three different categories: (the onset of CCFL, (the partial liquid delivery, and (r) the zero liquid penetration. The observed mechanisms of the onset of CCFL were different depending on the inlet water flow rate. The parametric effects of pipe diameter, horizontal pipe length, horizontal pipe length-to-diameter (L/D) ratio, and initial water level in the horizontal pipe of the test section on the onset of air-water CCFL were also examined. An empirical correlation for the onset of CCFL in a horizontal pipe connected to an inclined riser was developed in terms of Wallis flooding parameters for the low inlet water flow rate region. Comparisons of the present empirical correlation with the air-water CCFL data of large pipe diameters show that the present correlation agrees more closely with the experimental data than the existing CCFL correlations.

Key Words : countercurrent flow limitation (CCFL), flooding, hot leg, dimensionless superficial velocity, hydraulic jump, roll wave, onset of CCFL

1. Introduction

The phenomenon of countercurrent flooding has already been extensively studied for more than 30 years both experimentally and theoretically, but most of the existing studies on flooding were focused on vertical[1-5] and horizontal[6-8] pipes with a small diameter of less than 0.10 m.

The most widely used flooding correlation for vertical channel has been the Wallis[1] correlation, which characterizes a balance of inertia forces and hydrostatic forces:

$$j_G^{*\,0.5} + m j_L^{*\,0.5} = c \qquad (1)$$

where

$$j_K^* = j_K \left[\frac{\rho_K}{gD(\rho_L - \rho_G)} \right]^{0.5} \quad (2)$$

where j_K and ρ_K are the superficial velocities and densities of phase K (L = liquid phase and G = gas phase), D is the diameter of the pipe, and g is the gravitational acceleration. In Eq. (1), m and c are functions of channel entry geometric conditions ($m \cong 1.0$ and $c \cong 0.7 \sim 1.0$). Considering the limiting case of total flooding (j_L = 0, i.e., for zero liquid penetration), Kutateladze[2] has established analytically the following criterion:

$$Ku_K = j_K \left[\frac{\rho_K^2}{\sigma g(\rho_L - \rho_G)} \right]^{0.25} = 3.2 \quad (3)$$

where the dimensionless group Ku_K is known as the Kutateladze number and σ is the surface tension. Richer[3] noted that the Wallis correlation is more appropriate for small diameter channel, whereas Eq. (3) is applicable for relatively large diameter channels. Also, Tien et al.[4] proposed the following flooding correlation analogous to the Wallis correlation for vertical channels:

$$Ku_G^{0.5} + m_k Ku_L^{0.5} = c_k \quad (4)$$

They found that m_k and c_k varied with the channel entry geometry and $m_k \cong 0.65 \sim 0.8$ and $c_k = c_1 \tanh [c_2 D^{*0.25}]$ ($c_1 \cong 1.79 \sim 2.1$ and $c_2 \cong 0.8 \sim 0.9$), where D^* is a dimensionless pipe diameter given by

$$D^* = D \left[\frac{g(\rho_L - \rho_G)}{\sigma} \right]^{0.5} \quad (5)$$

Recently, Mcquillian and Whalley[5] summarized various vertical flooding data and existing correlations. As a conclusion, they found that the correlations that use dimensionless superficial velocities were not very successful, particularly at high liquid flow rates.

In a horizontal or nearly horizontal channel, the flow transition from stratified to slug flow has been identified as a cause of flooding. Wallis and Dobson[6] performed experimental and analytical studies of transition to slug flow in essentially horizontal rectangular channels with air and water at approximately atmospheric pressure: They suggested a relationship between the dimensionless air superficial velocity (jG*) and the average void fraction (α) for flow transition. Gardner[7] developed a criterion for flooding in the countercurrent flow of two fluids in horizontal tubes and channels. His experimental data confirmed the applicability of his modified model for flooding that was based on equations set up for lossless waves. He also found that the forms of water entry to the discharge tube (e.g., a sharp-edged entry or a bell-mouth entry) affect the flooding. Most recently, based on their visual observations, Choi and NO[8] suggested two mechanisms governing the transition to flooding in nearly horizontal pipes: "inner flooding" and "entrance flooding". The inner flooding is initiated by unstable wave growth, i.e., slugging, at the inner location of the pipe. The entrance flooding, on the other hand, is always observed to take place at the entrance of the water flow without slugging. They also found that a small deviation of the inclination angle from the horizontal plane ($0° < \theta < 1°$) causes a large deviation of the required air flow rates for flooding.

More recently, however, the countercurrent flooding in various pipe geometry, such as (1) vertical-to-horizontal, (2) vertical-to-inclined pipes containing elbows of varying angles, and (3) horizontal tube connected to an inclined riser has also been investigated[9-12]. The geometry of the bend that connects the horizontal pipe to an inclined riser, in particular, is analogous to that of a hot leg connecting the pressure vessel with the

steam generator in a pressurized water reactor (PWR).

Ohnuki[9] performed experiments to investigate the CCFL characteristics of air-water and saturated steam-water flow in a modeled flow path of a horizontal tube connected to an inclined riser. In his results, he firstly suggested a Wallis-type CCFL correlation applicable to an actual PWR hot leg. Siddiqui et al.[10] studied experimentally the effects of horizontal pipe length, bend radius of curvature, pipe diameter, entrance geometry, and slight inclination of horizontal leg on CCFL in pipe elbows consisting of an upper vertical leg and a lower leg that is horizontal or slightly inclined. Flooding, as observed in their experiments, appears to results from an unstable wave formation (slugging) at the hydraulic jump which forms in the lower pipe limb close to the bend. Kawaji et al.[11] also obtained countercurrent flooding data using air and water for vertical-to-downwardly inclined pipes containing elbows of varying angles. According to their observations, flooding in the vertical-to-horizontal pipe was found to be strongly affected by the formation of a hydraulic jump in the horizontal section near the elbow. This is in agreement with the Siddiqui's results. At moderate to high liquid flow rates or with short horizontal section, the hydraulic jump may be swept out of the horizontal pipe, and flooding will occur at significantly higher gas flow rates. Flooding in vertical-to-downwardly inclined pipes required higher gas flow rates than in vertical or vertical-to-horizontal pipes at low to moderate liquid flow rates ($jL^{*0.5} < 0.6$). Wongwises[12] observed that there are different mechanisms that lead to flooding depending on the liquid flow rate in a horizontal pipe with a bend: For low and intermediate liquid flow rates, the onset of flooding appears simultaneously with the slugging of unstable waves that are formed at the crest of the hydraulic jump. For high liquid flow rates, on the other hand, no hydraulic jump is observed, and flooding occurs as a result of slug formation at the end of the horizontal pipe. Their results show that the effects of the inclination angle of the bends, the liquid inlet conditions and the length of the horizontal pipes on the onset of CCFL are very significant.

In connection with the safety analysis of nuclear reactor systems, the most typical events where the countercurrent flow limitation (CCFL) can occur in the hot legs of PWRs are the reflood phase of a large break LOCA and the reflux cooling in a small break LOCA.

The main purpose of this work is to investigate the characteristics of CCFL in a horizontal pipe connected to an inclined riser by a 35 degree bend, which simulates the geometry of a PWR hot leg, and to examine the effects of various parameters such as (1) the pipe diameter, (2) the length of horizontal pipe, (3) the horizontal pipe length-to-diameter ratio, and (4) initial water level in the horizontal pipe of the test section on the CCFL. An empirical correlation for the CCFL in a PWR hot leg has also been presented.

2. Experiments

A series of experiments were performed and a total of 118 experimental data for the onset of CCFL and zero liquid penetration (105 for the onset of CCFL and 13 for the zero liquid penetration) in a simulated PWR hot leg have been obtained for various combinations of test parameters.

2.1. Experimental Apparatus

A schematic of the experimental apparatus is shown in Fig. 1(a). The experimental loop was designed to form a countercurrent flow in a test

Table 1. Test Section Geometry of the Present Experiments

Volume Reduction Ratio	Inner Pipe Diameter (D) (mm)	Horizontal Pipe Length (L) (mm)	Inclined Riser Length (l) (mm)	Inclination Angle (θ) (deg.)	Test Section Number
1 / 650	80	928 (*12)	623	35	No.1
		2000 (*25)			No.2
		3388 (*42)			No.3
			0		No.4
		3388 (*42)		0	No.5
1 / 3675	40	700 (*18)	648	35	No.6
		1000 (*25)			No.7
		3388 (*85)			No.8

* L/D Ratio

section. Water and air were used as the working fluids. The main components of the system were (a) the test section, (b) the air supply, (c) the water circulation system, and (d) the instrumentation and data acquisition system. A total of 8 different test sections (with different combinations of the pipe diameter, the horizontal pipe length, and the inclined riser as summarized in Table 1) were made of transparent acrylic glass to allow visual observation of the flow pattern. Each test section consisted of a horizontal pipe connected to an inclined riser by a 35(bend as shown in Fig. 1(b). The inner and outer radii of the curvature of the bend were 40 and 80 mm for the 40 mm bore pipe and 80 and 160 mm for the 80 mm bore pipe, respectively. The bends with different inner diameter were carefully constructed by bending straight acrylic glass pipes while they were heated on a machined die.

One end of the horizontal pipe was connected to the air vessel, while the other end of the inclined riser was connected to the water vessel. The air vessel had a cubic shape (600×600×1000 mm) and the water vessel had a rectangular cross-section (400×400mm) with 805 mm height. As can be seen in Fig. 1(a), the air vessel had a baffle plate to separate the vessel into two regions. This baffle plate is used to control the initial water level in the horizontal pipe of the test section by changing the height of the plate. The water vessel, on the other hand, had an inclined wall in the upper region to be connected to the inclined riser of the test section.

Air was supplied from the roots-type blower (whose capacity was 0~6000 LPM and the maximum operation pressure was 1.3 bar) to pass through the pressure regulator, rotameters (with two different ranges), the air vessel and the test section. The water was pumped from the constant head water surge tank and passed through the magnetic flowmeter, the water vessel, the test section, and two water collection tanks. Thus, the water flow was countercurrent to the air and formed a closed loop. The flow rates of water and air were controlled not only by adjusting motor controllers of the water pump and the air blower, but also by opening the bypass valves installed on each supply lines.

A digital video camera with a speed of 30 frames per second was also used to photograph

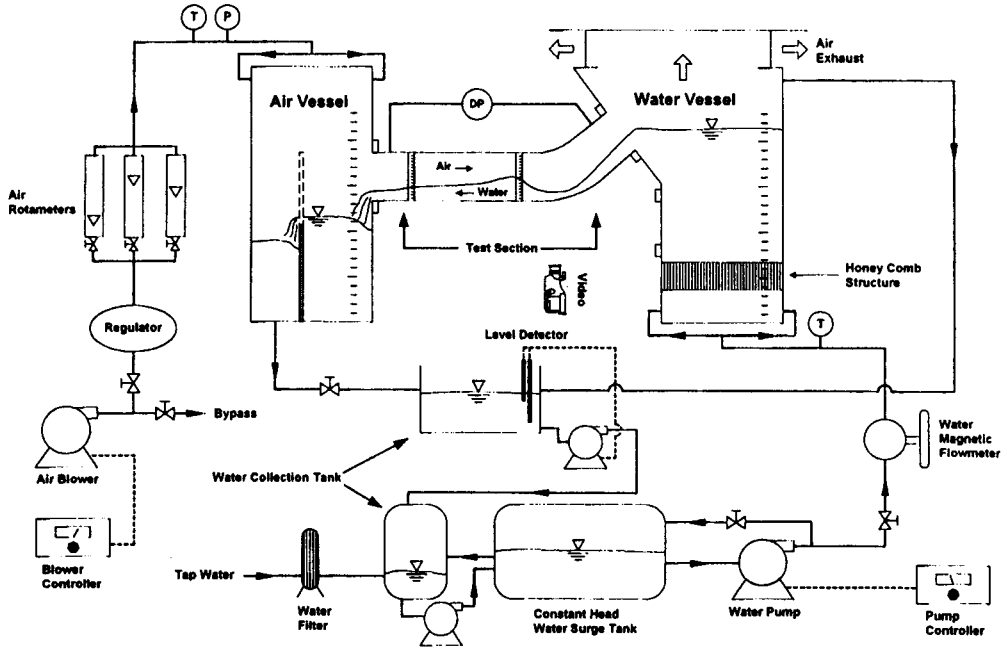

(a) Test Loop

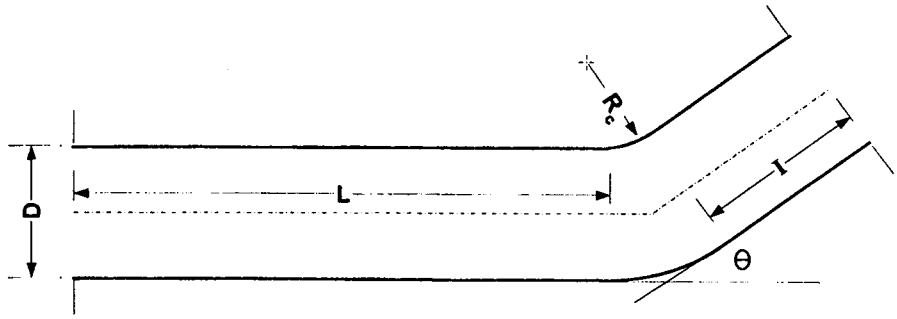

(b) Test Section

Fig. 1. Schematic Diagram of Experimental Apparatus

the flow pattern in the test section. A Hewlett Packard 3852A data acquisition unit (DAU) was used to process the output signals of transducers and compensated type-K thermocouples. The Pentium processor PC controlled the HP 3852A DAU and recorded the data in the hard disk. Communication between the PC and the HP 3852A DAU was carried out via the HP-IB interface card.

2.2. Test Parameters & Test Procedure

The controllable test parameters in the present work were (a) the pipe diameter, (b) the length of horizontal pipe, (c) the length of inclined riser, (d) the initial water level in the horizontal pipe of the test section, and (e) the inlet flow rate of water. A total of 118 runs were made for various combinations of test parameters using 8 different

Table 2. Test Matrix of the Present Experiments

Test Section	Water Flow Rate (LPM)	Air Flow Rate (LPM)	jL (m/s)	jG (m/s)	Test No. Data	No. of
No.1 No.2 No.3 No.4 No.5	1, 3, 6, 11, 17, 24, 33, 43, 54, 67, 81, 96, 113	100~2800 1 Step : 25	0.0033 ~0.3747	0.3316 ~9.2840	No.1-1 ⋮	88
No.6 No.7 No.8	1, 2, 3, 4, 6, 8, 10, 12, 14, 17	60~460 1 Step : 10	0.0133~ 0.2255	0.7958~ 6.1009	No.6-1 ⋮	130
Total Number of Experimental Data						**118**

test sections under atmospheric pressure and room temperature conditions as summarized in Table 2. The ranges of superficial velocities of water and air (i.e., j_L and j_G) were 0.0133~0.2255 m/s and 0.7958~6.1009 m/s for the 40 mm diameter pipe and 0.0033~0.3747 m/s and 0.3316~9.2840 m/s for the 80 mm diameter pipe, respectively.

The experimental procedure with a given test section is as follows: (a) The initial water level in the horizontal pipe of the test section was first set to a specified value. (b) Next, the inlet water flow rate was set to a specified value. (c) The air flow rate was then increased in small steps until the onset of CCFL or the zero liquid penetration limit occurred depending on the purpose of the test. (d) The void fraction was also measured at the point where the water depth was highest concurrently with each step of the air flow rate. The onset of CCFL was readily determined by visual observation as a slight increase in air flow rate (at the onset of CCFL) resulted in a dramatic change in the flow pattern and it was also confirmed by the sudden increment of pressure drop measured across the test section. In addition, the reproducibility of the present test data has been confirmed by repeating the same test three times under typical test conditions. All experiments, except for the tests conducted to examine the effects of the initial water level in the horizontal pipe of the test section, were performed under the free falling condition of the water at the water outlet.

3. Results and Discussion

3.1. Three Categories of CCFL and CCFL Mechanisms Observed in Three Different Regions of Inlet Water Flow Rates

3.3.1. Three Categories of CCFL

Figure 2 shows the major characteristic of pressure drop measured across the test section when the onset of CCFL occurred. According to the water flow rate that can exist in the test section for a given inlet water flow rate, the CCFL phenomenon can be classified into three different categories as shown in Fig. 3: ① the onset of CCFL, ② the partial delivery of water, and ③ the zero liquid penetration. As can be seen in Fig. 3, the point where the onset of CCFL occurred (i.e., the $j_G^{*0.5}$ value for a given $j_L^{*0.5}$ denoted by a dotted line in Fig. 3) varies depending on the inlet water flow rate. The zero liquid penetration limit for a

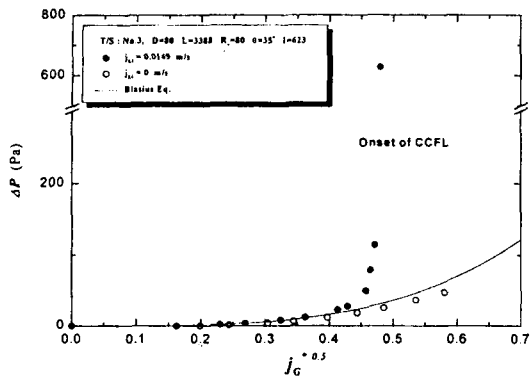

Fig. 2. Relationship between Pressure Drop and Air Flow Rate at Constant Inlet Water Flow Rate

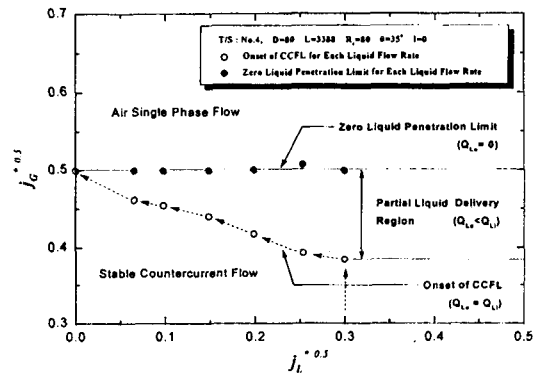

Fig. 3. Three Categories of CCFL

given inlet water flow rate (denoted by small black circles on a solid line in Fig. 3), on the other hand, is almost constant implying that the zero liquid penetration limit is independent of the inlet water flow rate.

3.1.2. Onset of CCFL Mechanisms Observed in Three Different Regions of Inlet Water Flow Rates

Figure 4 is a typical onset of CCFL curve (obtained with Test Section No.2: L=2000 mm, D=80 mm, Inclined Riser Legnth=623 mm, and θ =35°) expressed in terms of Wallis flooding

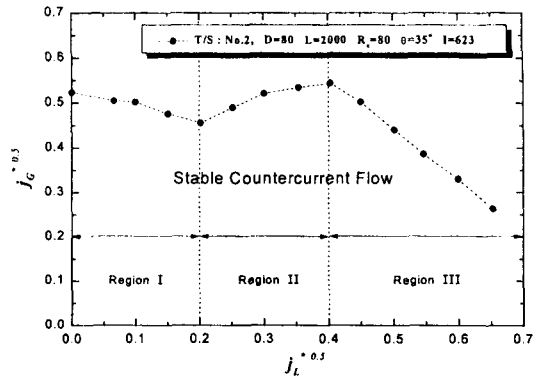

Fig. 4. Typical Onset of CCFL Curve

parameter ($j_K^{*0.5}$) defined by Eq. (2)

It may be recalled here that in an open channel flow, flows at depths greater than critical are known as subcritical flows; flows at depths less than critical are known as supercritical flows. When a change from supercritical to subcritical flow occurs in an open channel flow, a hydraulic jump appears. As a result, the water depth increases abruptly in the direction of flow. Although the expression that corresponds to the critical flow condition for stratified two-phase flow is different from that applicable to an open channel flow, the same terms are used to describe the stratified two-phase flow in the following.

As shown in Fig. 4, the CCFL curve can be divided into three regions based on the range of the inlet water flow rate (or equivalently, $jL^{*0.5}$). The observed mechanisms of CCFL in each region were different depending on the inlet water flow rate as follows:

1) In the low inlet water flow rate region (Region I: $0 < jL^{*0.5} < 0.2$), the air flow rate to initiate the onset of CCFL decreased as the inlet water flow rate was increased. Due to the acceleration of water by gravity while flowing down through the inclined pipe, the supercritical flow suddenly changes to the

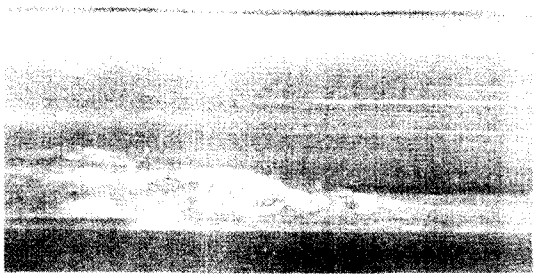

Fig. 5. Hydraulic Jump in the Horizontal Pipe ($j_L^{*0.5} < 0.2$)

Fig. 6. Water Hold up at the Bend When Onset of CCFL Occurs ($j_L^{*0.5} < 0.2$)

subcritical flow at a certain location in the horizontal pipe and a hydraulic jump occurred at the flow transition point as shown in Fig. 5. The location of the hydraulic jump depended on the water flow rate: When the inlet water flow rate was decreased, the location of the hydraulic jump moved closer to the bend. As the inlet water flow rate was increased, the hydraulic jump moved away from the bend and the magnitude of hydraulic jump was also increased. Also, as the air flow rate was increased for a given inlet water flow rate, the hydraulic jump moved toward the bend and the air-water interface became very wavy. When the hydraulic jump arrived near the bend, the flow pattern became chaotic and oscillatory, and large roll waves were also observed at the air-water interface near the bend. Figure 6 shows the flow pattern observed in the vicinity of the bend when the

Fig. 7. The Large Roll Wave Formation at the Outlet of Water ($0.2 < j_L^{*0.5} < 0.4$)

CCFL occurred.

2) In the intermediate inlet water flow rate region (Region II: $0.2 < jL^{*0.5} < 0.4$), the air flow rate to initiate the onset of CCFL increased as the inlet water flow rate was increased. The accelerated water flowing down through the inclined pipe connected by a 35° bend maintained a supercritical flow throughout the horizontal pipe and no hydraulic jump occurred within the pipe. When the air flow rate reached the point of the onset of CCFL, the depth of water layer increased at the horizontal pipe outlet. At the same time, a large number of small water droplets were entrained in the upper region of the pipe from the air-water interface and also large amplitude roll waves were developed near the horizontal pipe outlet as can be seen in Fig. 7. These roll waves were moved quickly toward the bend by the flowing air. This, in turn, increased the velocity of air because of the decrease of the effective cross-sectional area of air flow by the roll waves. As a result of the increased air flow velocity, the water flow rate was eventually restricted.
3) In the high inlet water flow rate region (Region III: $0.4 < j_L^{*0.5} < 0.7$), the air flow rate to initiate the onset of CCFL decreased as the inlet water flow rate was increased and it was independent

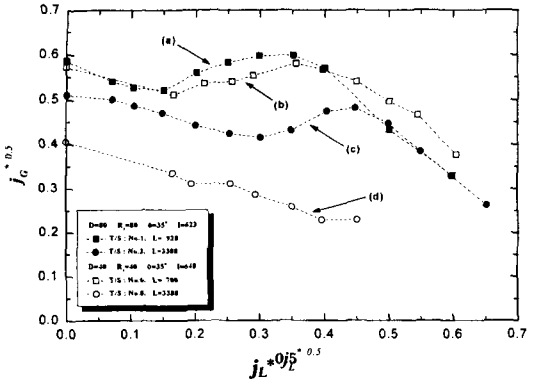

Fig. 8. Effect of Pipe Diameter on CCFL

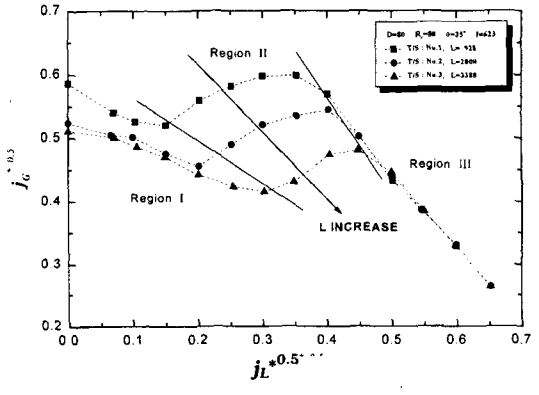

Fig. 9. Effect of Horizontal Pipe Length on CCFL

of the test section geometry for a given pipe diameter. In the region III, there was no hydraulic jump in the horizontal pipe and also there was no increase of water layer depth at the horizontal pipe outlet. However, the onset of CCFL occurred at the inlet of the inclined pipe connected to the water vessel due to an active entrainment of water droplets into the water vessel.

It should be noted, however, the above quantitative criteria used to define the three different regions of the inlet water flow rate are not directly applicable to other test sections with a different combination of pipe geometry such as L, D, and L/D.

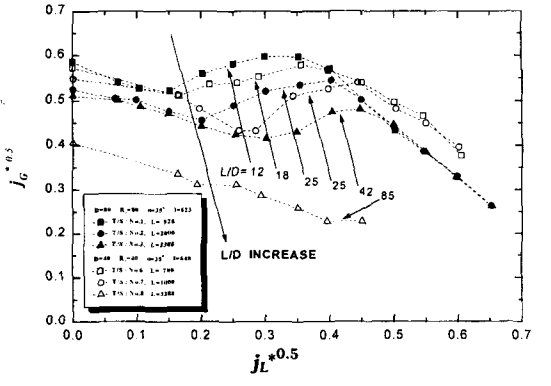

Fig. 10. Effect of Horizontal Pipe Length-to-Diameter Ratio on CCFL

3.2. Effects of Various Geometrical Parameters on CCFL

3.2.1. Pipe Diameter Effect on CCFL

To examine the effect of the pipe diameter on the CCFL, experimental data obtained with four different combinations of pipe diameter and horizontal pipe length are plotted in Fig. 8. A comparison between curves (a) and (b) shows that the effect of pipe diameter on the onset of CCFL for short horizontal pipes (L = 928 and 700 mm) is not clear. For longer horizontal pipes (L =3388 mm), curves (c) and (d), on the other hand, $j_G^{*0.5}$ values to initiate the onset of CCFL for smaller pipe diameter (D = 40 mm) are much smaller than that for larger pipe diameter (D = 80 mm) for a given value of $jL^{*0.5}$.

3.2.2. Horizontal Pipe Length Effect on CCFL

The CCFL data obtained with test sections of three different horizontal lengths are shown in Fig. 9. This figure clearly shows that a longer horizontal pipe length leads to lower velocities of air and water for the onset of CCFL, which agrees with the results of others. As already pointed out by earlier workers[9,10,12], the longer horizontal

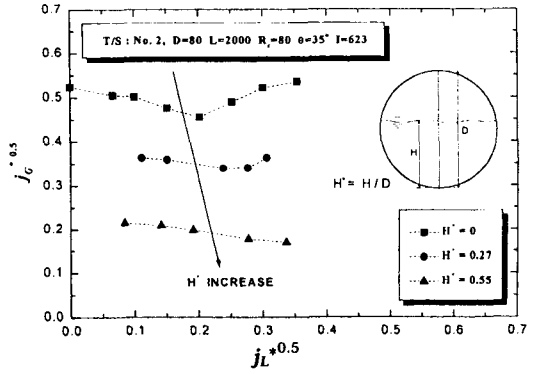

Fig. 11. Effect of Stagnant Water in the Test Section on the Onset of CCFL

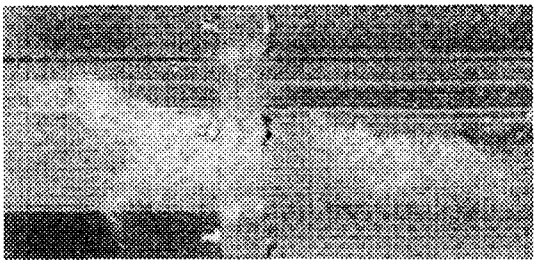

Fig. 12. Hydraulic Jump in the Presence of Stagnant Water in the Horizontal Pipe ($j_L^{*0.5}$=0.34)

pipe lengths cause the water level to be higher in the vicinity of the bend due to an increase in frictions at the wall and interface and slows down the water flow. This, in turn, induces a higher gas velocity and hence an earlier formation of unstable wave growth at the hydraulic jump.

3.2.3. Length-to-Diameter Ratio (L/D) Effect on CCFL

To examine the effect of the horizontal pipe length-to-diameter ratio, flooding parameters, $jL^{*0.5}$ versus $jG^{*0.5}$, are plotted using L/D as a major parameter in Fig. 10. This figure also shows that a larger L/D leads to lower velocities of air and water for the onset of CCFL. That is, the onset of CCFL occurs at consistently lower flow rates when the L/D is increased. Since a larger L/D corresponds to a longer horizontal pipe length for a given pipe diameter, the same reasoning used in the horizontal length effect on the CCFL is applicable.

3.3. Effect of Initial Water Level in the Horizontal Pipe of the Test Section on CCFL

For a given inlet water flow rate and a given test section, the onset of CCFL occurred at much lower air flow rate when the lower part of the horizontal pipe of the test section was initially filled with stagnant water than without initial water level build-up in the test section (i.e., the free falling condition for the condensate). Figure 11 shows $j_L^{*0.5}$ versus $j_G^{*0.5}$ curves for three dimensionless water depths. As can be seen in this figure, the air flow rate for the onset of CCFL decreases as the initial water level is increased for a given inlet water flow rate. This phenomenon results from the following reasons: (1) The presence of stagnant water in the horizontal pipe of the test section naturally elevates the water level throughout the horizontal pipe as well as in the vicinity of the bend. (2) Also the stagnant water in the horizontal pipe effectively slows down the accelerated water flowing through the inclined pipe by gravity. As a result, a hydraulic jump can be generated in the horizontal pipe close to the bend. In addition, as can be seen in Fig. 12, the magnitude of the hydraulic jump originated from the sudden deceleration of the flow velocity caused by any obstacle in the flow conduit (e.g., stagnant water in this case) is higher than that generated without it. The increased magnitude of the hydraulic jump, in turn, raises the water level in the vicinity of the bend. As already pointed out in the description of the horizontal pipe length effect on CCFL, the higher water level in the vicinity of the bend induces a higher gas velocity and hence an

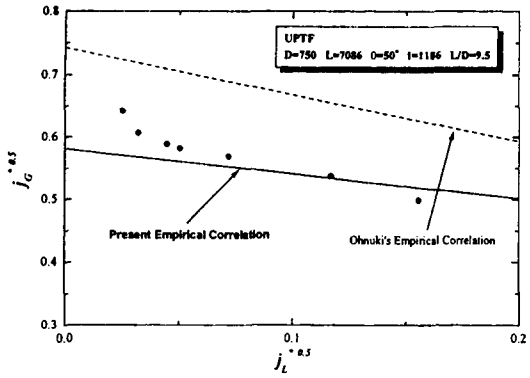

Fig. 13. Comparison of the Present Correlation with the UPTF Data

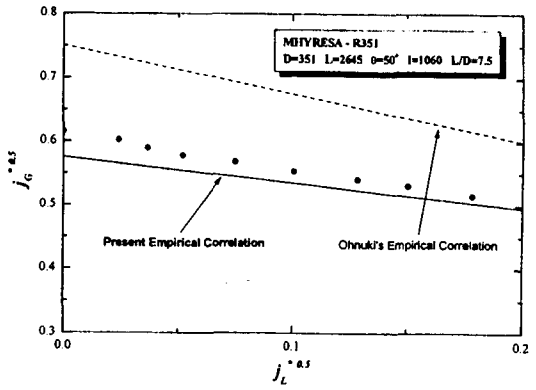

Fig. 14. Comparison of the Present Correlation with the MHYRESA-R351 Data

earlier formation of unstable wave growth at the hydraulic jump. All of these phenomena add together to bring an earlier occurrence of the onset of CCFL.

3.4. Empirical Correlation for the Onset of CCFL in Low Inlet Water Flow Rate Region

3.4.1. Development of Empirical Flooding Correlation

Using the present experimental data obtained for the low inlet water flow rate region (a total of 19 points from 4 test sections , $0 < j_L^{*0.5} < 0.2$), an empirical correlation for the onset of CCFL in a simulated PWR hot leg has been developed in terms of water and air Wallis flooding parameters (jK(0.5) using a linear relationship between the two parameters as follows:

$$j_G^{*0.5} + 0.397 j_L^{*0.5} = 0.603 - 0.00234\left(\frac{L}{D}\right) \quad (6)$$

The present as well as the previous studies show that not only all the geometric parameters used in Eq. (6) (i.e., horizontal pipe length, L and diameter, D) but also the inclined riser length, I, affects the onset of CCFL. The inclined riser of the test sections used in the present experiments, in particular, were designed to have the same hydraulic head of the Korea standard nuclear power plant (KSNPP, ULCHIN 3&4). The quantitative relation between the onset of CCFL and inclined riser length has not been incorporated in the present empirical correlation. However, in the case of a sufficiently long inclined riser, it is possible that there is a certain saturation point where the inclined riser length no longer affects the onset of CCFL. Regarding the possible existence of the saturation length of the inclined riser, further researches are needed in the future.

3.4.2. Comparisons of the Empirical Correlation with Existing Data

Comparisons of the present empirical correlation with existing data obtained with large pipe diameters (D (351 mm), in particular, have been made in the low inlet water flow rate region. Comparisons of the present and Ohnuki's empirical correlations[9] with the existing experimental data for the air-water CCFL in a

simulated PWR hot leg of UPTF[13] and MHYRESA[14] are made in Figs. 13 and14. All the relevant geometry of the test sections used in the above two experiments were used to predict the onset of CCFL with the present and Ohnuki's correlations. These figures show that the present empirical correlation agrees with the large pipe diameter data more closely than Ohnuki's empirical correlations in the low inlet water flow rate region. In general, the present empirical correlation underpredicts the existing experimental data. The reason for this may be partly due to the sharp edge of water inlet of the present test sections that enhances the initial flow instability of water flowing into the test sections, which, in turn, leads to the onset of CCFL condition at a lower air flow rate for a given inlet water flow rate.

4. Conclusions

The air-water CCFL in a simulated PWR hot leg has been experimentally investigated. The results of present experiments can be summarized as follows:

1) A total of 118 experimental data for the air-water CCFL (i.e., 105 for the onset of CCFL and 13 for the zero liquid penetration) have been obtained for various combinations of test parameters.
2) According to the water flow rate that can exist in the test section for a given inlet water flow rate, the CCFL phenomenon can be classified into three different categories: ① the onset of CCFL, ② the partial liquid delivery, and ③ the zero liquid penetration.
3) Three different mechanisms of the onset of CCFL were observed depending on the inlet water flow rate.
4) The effects of geometrical parameters, such as the pipe diameter, the length of horizontal pipe, and the horizontal pipe length-to-diameter (L/D) ratio, and operating condition of initial water level in the test section on the onset of CCFL were also examined.
5) On basis of the present experimental data in low inlet water flow rate region, an empirical correlation for the onset of CCFL in a simulated PWR hot leg has been developed in terms of water and air Wallis flooding parameters ($j_K^{*0.5}$) using a linear relationship.
6) Comparisons of the present as well as the existing correlations with the air-water CCFL data of large pipe diameters show that the present correlation agrees more closely with the data than the existing correlations[9].

Nomenclature

c	y-intercept of the Wallis-type CCFL curve
c_k	y-intercept of the Tien-type CCFL curve
D	diameter of pipe, mm
D*	dimensionless pipe diameter
g	acceleration of gravity, m/s^2
H	water depth, mm
H*	dimensionless water depth
I	length of upwardly inclined pipe, mm
j_K	superficial velocity of K phase, m/s
j_K^*	dimensionless superficial velocity of K phase
Ku_K	Kutateladze number of K phase
L	length of horizontal pipe, mm
m	slope of the Wallis-type CCFL curve
m_k	slope of the Tien-type CCFL curve
R_c	radius of curvature, mm

Greek

α	average void fraction
θ	inclination angle, °
ρ	density, kg/m^3
σ	surface tension, N/m

Subscripts

G gas phase ; air
i inlet
K phase of fluid; liquid or gas
L liquid phase ; water
o outlet

Acknowledgement

The authors gratefully acknowledge the financial support of Korea Electric Power Research Institute (KEPRI) provided for this work.

References

1. G. B. Wallis, One-Dimensional Two-Phase Flow, p. 408, McGraw-Hill Book Company, New York (1969).
2. S. S. Kutateladze, "Elements of the Hydrodynamics of Gas-Liquid Systems," *Fluid Mech.-Sov. Res.*, **1** (4), 29 (1972).
3. H. J. Richter, "Flooding in Tubes and Annuli," *Int. J. Multiphase Flow*, **7** (6), 647 (1981).
4. C. L. Tien, K. S. Chung, and C. P. Liu, Flooding in Two-Phase Countercurrent Flows, EPRI / NP-1283 (1979).
5. K. W. Mcquillan and P. B. Whalley, "A Comparison between Flooding Correlations and Experimental Flooding Data for Gas-Liquid Flow in Vertical Circular Tubes," *Chem. Eng. Sci.*, **40** (8), 1425 (1985).
6. G. B. Wallis and J. E. Dobson, "The Onset of Slugging in Horizontal Stratified Air-Water Flow," *Int. J. Multiphase Flow*, **1**, 173 (1973).
7. G. C. Gardner, "Flooded Countercurrent Two-Phase Flow in Horizontal Tubes and Channels," *Int. J. Multiphase Flow*, **9** (4), 367 (1983).
8. K. Y. Choi and H. C. No, "Experimental Studies of Flooding in Nearly Horizontal Pipes," *Int. J. Multiphase Flow*, **21** (3), 419 (1995).
9. A. Ohnuki, "Experimental Study of Counter-Current Two-Phase Flow in Horizontal Tube Connected to Inclined Riser," *J. Nucl. Sci. Tech.*, **23** (3), 219 (1986).
10. H. Siddiqui, S. Banerjee, and K. H. Ardron, "Flooding in an Elbow Between a Vertical and a Horizontal or Near-Horizontal Pipe," *Int. J. Multiphase Flow*, **12** (4), 531 (1986).
11. M. Kawaji, L. A. Thomson, and V. S. Krisnan, "Countercurrent Flooding in Vertical-to-Inclined Pipes," *Exp. Heat Transfer*, **4**, 95 (1991).
12. S. Wongwises, "Two-Phase Countercurrent Flow in a Model of a Pressurized Water Reactor Hot Leg," *Nucl. Eng. Des.*, **166**, 121 (1996).
13. M. J. Dillstone, Analysis of the UPTF Separate Effects Test 11 (Steam-Water Countercurrent Flow in the Broken Loop Hot Leg) Using RELAP5/MOD2, NUREG / IA-0071 (1992).
14. G. Geffraye, P. Bazin, P. Pichon, and A. Bengaouer, "CCFL in Hot Legs and Its Prediction with the CATHRE Code," Proc. 7th Int. Meeting on Nuclear Reactor Thermal Hydraulics, NURETH-7, Saratoga Springs, New York (1995).